Journal of Theoretical Biology 558 (2023) 111353

Contents lists available at ScienceDirect

Journal of Theoretical Biology

journal homepage: www.elsevier.com/locate/yjtbi

Exploring the role of superspreading events in SARS-CoV-2 outbreaks

Jordan Bramble [a], Alexander Fulk [b], Raul Saenz [c], Folashade B. Agusto [b,*]

[a] Department of Mathematics, University of Kansas, Lawrence, KS, United States of America
[b] Department of Ecology and Evolutionary Biology, University of Kansas, Lawrence, KS, United States of America
[c] Department of Population Health, University of Kansas Medical Center, Kansas City, KS, United States of America

ARTICLE INFO

Keywords:
SARS-CoV-2
Superspreading events
Human behavior
Continuous-time Markov chain
Gillespie's direct algorithm

ABSTRACT

The novel coronavirus SARS-CoV-2 emerged in 2019 and subsequently spread throughout the world, causing over 600 million cases and 6 million deaths as of September 7th, 2022. Superspreading events (SSEs), defined here as public or social events that result in multiple infections over a short time span, have contributed to SARS-CoV-2 spread. In this work, we compare the dynamics of SSE-dominated SARS-CoV-2 outbreaks, defined here as outbreaks with relatively higher SSE rates, to the dynamics of non-SSE-dominated SARS-CoV-2 outbreaks. To accomplish this, we derive a continuous-time Markov chain (CTMC) SARS-CoV-2 model from an ordinary differential equation (ODE) SARS-CoV-2 model and incorporate SSEs using an events-based framework. We simulate our model under multiple scenarios using Gillespie's direct algorithm. The first scenario excludes hospitalization and quarantine; the second scenario includes hospitalization, quarantine, premature hospital discharge, and quarantine violation; and the third scenario includes hospitalization and quarantine but excludes premature hospital discharge and quarantine violation. We also vary quarantine violation rates. Results indicate that, with either no control or imperfect control, SSE-dominated outbreaks are more variable but less severe than non-SSE-dominated outbreaks, though the most severe SSE-dominated outbreaks are more severe than the most severe non-SSE-dominated outbreaks. We measure severity by the time it takes for 50 active infections to be achieved; more severe outbreaks do so more quickly. SSE-dominated outbreaks are also more sensitive to control measures, with premature hospital discharge and quarantine violation substantially reducing control measure effectiveness.

1. Introduction

Severe acute respiratory syndrome coronavirus 2 (SARS-CoV-2) is the causative agent of COVID-19. As of September 7th, 2022, it has caused over 600 million cases and 6 million deaths worldwide (World Health Organization, 2022). Of those, over 84 million cases and 1 million deaths have occurred in the United States of America (Centers for Disease Control and Prevention, 2022). COVID-19 has strained the healthcare system, with many hospitals nearing or exceeding capacity (Alltucker and Bajak, 2020; Gabbat and Laughland, 2022; Hubbard, 2022; McCarthy, 2020). In response, both national and state-level governments have issued guidelines and mandates aimed at reducing transmission, ranging from social-distancing guidelines and mask mandates to stay-at-home orders and limits on large gatherings (MultiState Policy Team, 2021; Our World in Data, 2020).

The effectiveness of these guidelines and mandates has been hindered by imperfect adherence and compliance. For example, some people refuse to wear a mask (Haischer et al., 2020). Moreover, many people fail to social distance, despite doing so initially (Hoeben et al., 2021). People also violate stay-at-home orders, with several being issued citations and some being arrested (Hernandez, 2020; Knight, 2020; KSTP, 2020; West Hawaii Today Staff, 2020). Beyond refusing to mask, failing to social distance, and violating stay-at-home orders, some people voluntarily attend public or social events. Others may be forced to work in close proximity to each other, an example being workers in certain meat-packing plants (Pokora et al., 2021). Both of the aforementioned facilitate superspreading events (SSEs), defined here as public or social events that result in multiple infections over a short time span. Such events have contributed to the fast spread of SARS-CoV-2 (Swinkels, 2020; Althouse et al., 2020; Du et al., 2022; Lakdawala and Menachery, 2021). There are other settings that can facilitate SSEs, such as prisons, but these are not considered here (Althouse et al., 2020).

SSEs differ from superspreading individuals (SIs), which we define here as individuals who cause disproportionately more infections over their infectious lifetime. Event- and individual-based superspreading are not mutually exclusive; people who cause SSEs may qualify as SIs. However, this is not always the case. People may cause multiple

* Corresponding author.
E-mail address: fbagusto@gmail.com (F.B. Agusto).

https://doi.org/10.1016/j.jtbi.2022.111353
Received 30 June 2022; Received in revised form 31 October 2022; Accepted 7 November 2022
Available online 14 November 2022

infections at a public/social event but not cause disproportionately more infections over their infectious lifetime. Likewise, not all who become SIs do so by causing SSEs. Given that event- and individual-based superspreading are not mutually exclusive, factors relevant to SSEs are often relevant to SIs and vice versa. Intrinsic factors that potentiate superspreading (in general) include greater-than-average viral shedding and contact rates (Althouse et al., 2020; Lloyd-Smith et al., 2005; Chen et al., 2021); heterogeneity in SARS-CoV-2 shedding is evident in Badu, et al.'s literature review (Badu et al., 2021) on SARS-CoV-2 viral loads, shedding, and transmission dynamics. Extrinsic factors include crowding and poor ventilation (Althouse et al., 2020; Chen et al., 2021; Ashworth, 2021). Despite SSEs' and SIs' non-mutual exclusivity, they differ in that only a subset of the population may achieve SI status without causing SSEs, whereas anyone may cause SSEs under the right circumstances.

Event- and individual-based superspreading are incorporated into models using different frameworks. SSEs may be modeled via rare events resulting in multiple infections; these events may be caused by any individual, and their frequency and number of resulting infections each follow some distribution. This is the approach taken by James et al. (2007). SIs may be modeled via heterogeneity in infectivity; individual infectivity follows some distribution, the right tail of which corresponds to superspreader individuals. This is the approach taken by Lloyd-Smith et al. (2005). There are many other approaches to modeling SIs in the literature (Lakdawala and Menachery, 2021; Mushanyu et al., 2022; Ndaïrou et al., 2020; Shakiba et al., 2021); note that while some of these articles mention superspreading events, their frameworks are nonetheless individual-based. Despite the importance of superspreading in SARS-CoV-2 outbreaks being well-established (Swinkels, 2020; Althouse et al., 2020; Du et al., 2022; Lakdawala and Menachery, 2021), most SARS-CoV-2 models do not incorporate it. Of those that do, most utilize an individual-based framework (Lakdawala and Menachery, 2021; Mushanyu et al., 2022; Ndaïrou et al., 2020). Moreover, most superspreading-incorporating SARS-CoV-2 models do not include control measures (Mushanyu et al., 2022; Ndaïrou et al., 2020). SSEs' influence on SARS-CoV-2 outbreak dynamics – beyond being known contributors – is thus relatively unexplored from a modeling perspective, especially in the context of control. Wilasang et al. (2022) successfully reconstructed the first wave of SARS-CoV-2 transmission in Thailand using a superspreading-incorporating SARS-CoV-2 model with control, but they utilized an individual-based framework and included only one type of control. We utilize an events-based framework and include two types of control; to our knowledge, we are the only authors to do so.

In what follows, SSE-dominated outbreaks refer to outbreaks with relatively higher SSE rates than non-SSE-dominated outbreaks; non-SSEs refer to non-SSE-related infection events. The goals of this study are to investigate:

G1. The influence of SSEs relative to that of non-SSEs on outbreak dynamics
G2. The effectiveness of hospitalization and quarantine as control measures for SSE- versus non-SSE-dominated outbreaks
G3. The influence of quarantine violation on the effectiveness of quarantine for SSE- versus non-SSE-dominated outbreaks

We incorporate SSEs into a continuous-time Markov chain (CTMC) model, impose a constancy condition, and vary SSE and non-SSE rates to accomplish G1. The constancy condition requires that the expected number of infections following the CTMC model's first change in state remain constant for different SSE and non-SSE rates. We simulate the CTMC model under multiple scenarios to accomplish G2:

(i). With neither hospitalization nor quarantine (NHQ). This scenario excludes hospitalization and quarantine.
(ii). With realistic hospitalization and quarantine (RHQ). This scenario includes hospitalization, quarantine, premature hospital discharge, and quarantine violation.
(iii). With idealistic hospitalization and quarantine (IHQ). This scenario includes hospitalization and quarantine but excludes premature hospital discharge and quarantine violation.

Finally, we simulate the CTMC model under RHQ with varying levels of quarantine violation to accomplish G3. Our methods, results, and discussion are located in Sections 2, 3, and 4.

2. Methods

We derive our continuous-time Markov chain (CTMC) model from Agusto et al.'s (2022) baseline COVID-19 model (see Section 2.1) and incorporate SSEs in Section 2.2. The constancy condition is derived in Section 2.3. After formulating the CTMC model and imposing the constancy condition, we detail our simulation protocol in Section 2.4. Finally, we introduce two superspreading-incorporating, discrete-time Markov chain (DTMC) models from literature (Lloyd-Smith et al., 2005; James et al., 2007) in Section 2.5. These models' results are used for comparison in Section 4.

2.1. Baseline COVID-19 model

In Agusto, et al.'s baseline COVID-19 model (Agusto et al., 2022), the evolution of susceptible ($S(t)$), exposed ($E(t)$), asymptomatic ($A(t)$), symptomatic ($I(t)$), hospitalized ($H(t)$), quarantined ($Q(t)$), and removed ($R(t)$) individuals through time is governed by the system of ordinary differential equations given below:

$$\begin{aligned}
\frac{dS}{dt} &= -\beta\frac{S(t)[I(t)+\eta_A A(t)+\eta_Q Q(t)+\eta_H H(t)]}{N(t)},\\
\frac{dE}{dt} &= \beta\frac{S(t)[I(t)+\eta_A A(t)+\eta_Q Q(t)+\eta_H H(t)]}{N(t)} - \sigma E(t),\\
\frac{dA}{dt} &= q\sigma E(t) - (\gamma_A+\delta_A)A(t),\\
\frac{dI}{dt} &= (1-q)\sigma E(t) + \nu_Q Q(t) + \nu_H H(t) - (\omega_Q+\omega_H+\gamma_I+\delta_I)I(t),\\
\frac{dH}{dt} &= \omega_H I(t) - (\nu_H+\gamma_H+\delta_H)H(t),\\
\frac{dQ}{dt} &= \omega_Q I(t) - (\nu_Q+\gamma_Q+\delta_Q)Q(t),\\
\frac{dR}{dt} &= (\gamma_A+\delta_A)A(t) + (\gamma_I+\delta_I)I(t) + (\gamma_Q+\delta_Q)Q(t) + (\gamma_H+\delta_H)H(t).
\end{aligned} \tag{1}$$

The exposed and asymptomatic classes account for the virus' incubation period and the reduced infectiousness of asymptomatic individuals. Meanwhile, hospitalization and quarantine function as control measures. Movement of individuals from the hospitalized and quarantined classes back to the symptomatic class account for limited resources and human behavior. We refer to the former as premature hospital discharge and the latter as quarantine violation. The model's flow diagram is displayed in Fig. 1, and its parameters are defined in Table 1.

2.2. Continuous-time Markov chain model

We limit ourselves to outbreak scenarios – specifically, the short time period following the introduction of a small number of infected individuals into a completely susceptible population – so that we may assume the following:

(†) Population size and mixing is such that transmission events are independent of each other and unaffected by the depletion of susceptible individuals and accumulation of removed individuals (Miller, 2018).

This assumption is reasonable in outbreak scenarios because the number of infected individuals is small relative to the number of susceptible individuals. (†) implies that $\frac{S}{N} \approx 1$, so we may approximate the rate at which individuals transition from S to E due to non-SSEs as

$$\frac{\beta S(\eta_A A + I + \eta_Q Q + \eta_H H)}{N} \approx \beta(\eta_A A + I + \eta_Q Q + \eta_H H).$$

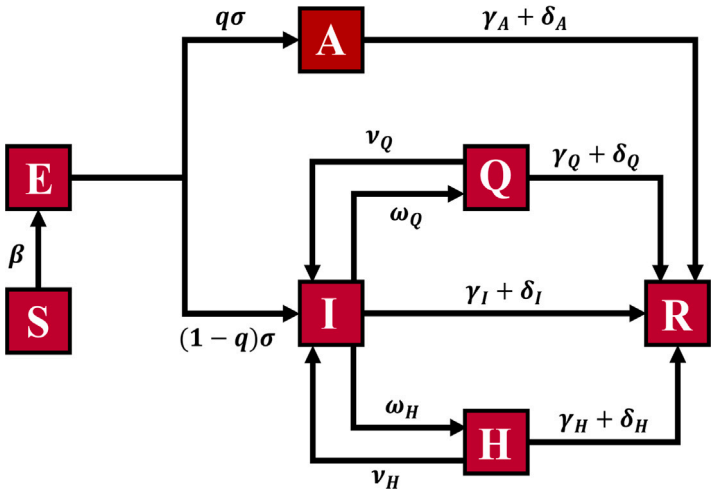

Fig. 1. Compartmental flow diagram for the baseline COVID-19 model (1). Susceptible individuals are exposed upon initial infection, and exposed individuals are either asymptomatic or symptomatic once infectious. Asymptomatic individuals are removed upon recovery or death, while symptomatic individuals may be hospitalized or quarantined and are removed upon recovery or death. Hospitalized and quarantined individuals may be prematurely discharged from the hospital or violate quarantine and are removed upon recovery or death.

Table 1
Parameter values for the baseline COVID-19 model (1).

Parameter	Description	Value	Sources
β	Infection rate	0.4975	Agusto et al. (2022), Edholm et al. (2022) and MIDAS Network (2021)
η_A, η_H, η_Q	Infection rate modifiers	0.45, 0.1362, 0.3408	Agusto et al. (2022, 2021)
q	Proportion that remain asymptomatic	0.5	Agusto et al. (2022, 2021) and Centers for Disease Prevention and Control (2020)
σ	Disease progression rate	$\frac{1}{6}$	Agusto et al. (2022) and Centers for Disease Prevention and Control (2020)
$\gamma_A, \gamma_I, \gamma_H, \gamma_Q$	Recovery rates	0.7565, 0.0775, 0.041, 0.083	Agusto et al. (2022), Cheng et al. (2020), Sanche et al. (2020), Johansson et al. (2021) and Renardy et al. (2020)
ω_H, ω_Q	Hospitalization & quarantine rates	0.1977, 0.453	Agusto et al. (2022, 2021)
ν_H, ν_Q	Hospital discharge & quarantine violation rates	0.1301, 0.4605	Agusto et al. (2022, 2021)
$\delta_A, \delta_I, \delta_H, \delta_Q$	Death rates	0.00325, 0.0065, 0.0065, 0.0065	Agusto et al. (2022, 2021) and UK Health Security Agency (2022)

The possible events corresponding to the baseline COVID-19 model (1) are:

$E_{S\to E} : S \to S-1, E \to E+1$ (An individual transitions from S to E)
$E_{E\to A} : E \to E-1, A \to A+1$ (An individual transitions from E to A)
$E_{A\to R} : A \to A-1, R \to R+1$ (An individual transitions from A to R)
$E_{E\to I} : E \to E-1, I \to I+1$ (An individual transitions from E to I)
$E_{I\to H} : I \to I-1, H \to H+1$ (An individual transitions from I to H)
$E_{I\to Q} : I \to I-1, Q \to Q+1$ (An individual transitions from I to Q)
$E_{I\to R} : I \to I-1, R \to R+1$ (An individual transitions from I to R)
$E_{H\to I} : H \to H-1, I \to I+1$ (An individual transitions from H to I)
$E_{H\to R} : H \to H-1, R \to R+1$ (An individual transitions from H to R)
$E_{Q\to I} : Q \to Q-1, I \to I+1$ (An individual transitions from Q to I)
$E_{Q\to R} : Q \to Q-1, R \to R+1$ (An individual transitions from Q to R)

$E_{S\to E}$ corresponds to a susceptible individual being exposed; $E_{E\to A}$ corresponds to an exposed individual becoming infectious but remaining asymptomatic; $E_{A\to R}$ corresponds to an asymptomatic individual recovering or dying; $E_{E\to I}$ corresponds to an exposed individual becoming infectious and symptomatic; $E_{I\to H}$ corresponds to a symptomatic individual being hospitalized; $E_{I\to Q}$ corresponds to a symptomatic individual being quarantined; $E_{I\to R}$ corresponds to a symptomatic individual recovering or dying; $E_{H\to I}$ corresponds to a hospitalized individual being prematurely discharged from the hospital; $E_{H\to R}$ corresponds to a hospitalized individual recovering or dying; $E_{Q\to I}$ corresponds to a quarantined individual violating quarantine; and $E_{Q\to R}$ corresponds to a quarantined individual recovering or dying.

Let $K \in \mathbb{N} \cup \{0\}$ be a Poisson random variable with expectation $\phi \in \mathbb{N}$. We incorporate SSEs by defining an additional event,

$$E_{SSE} : S \to S-k, E \to E+k \ (k \text{ individuals transition from S to E}),$$

where k is some possible value of K. E_{SSE} corresponds to k susceptible individuals becoming exposed. The event thus generates a random number of infections over a short period of time. This differs from $E_{S\to E}$, which generates one infection. In what follows, we take $\psi \in \mathbb{R}^+$ to be the deterministic rate at which infected individuals cause SSEs. (†) implies that SSEs involve a single infected individual and otherwise susceptible individuals, and assuming that hospitalized and quarantined individuals do not cause SSEs, we may take $\psi(\eta_A A + I)$ to be the deterministic rate at which SSEs occur.

Now, let $\tau \in \mathbb{R}^+$. By considering the above events' occurrence in a sufficiently small time interval, $(\tau, \tau + \Delta\tau)$, we may assume that at most one event occurs in this interval. The probabilities corresponding to each event's occurrence in $(\tau, \tau + \Delta\tau)$ are then:

$$P(E_{S\to E}; \Delta\tau) = \beta(\eta_A A + I + \eta_Q Q + \eta_H H)\Delta\tau, \qquad P(E_{SSE}; \Delta t) = \psi(\eta_A A + I)\Delta t,$$
$$P(E_{E\to A}; \Delta\tau) = q\sigma E\Delta\tau, \qquad P(E_{A\to R}; \Delta\tau) = (\gamma_A + \delta_A)A\Delta\tau,$$
$$P(E_{E\to I}; \Delta\tau) = (1-q)\sigma E\Delta\tau, \qquad P(E_{I\to H}; \Delta\tau) = \omega_H I\Delta\tau,$$
$$P(E_{I\to Q}; \Delta\tau) = \omega_Q I\Delta\tau, \qquad P(E_{I\to R}; \Delta\tau) = (\gamma_I + \delta_I)I\Delta\tau,$$
$$P(E_{H\to I}; \Delta\tau) = \nu_H H\Delta\tau, \qquad P(E_{H\to R}; \Delta\tau) = (\gamma_H + \delta_H)H\Delta\tau,$$
$$P(E_{Q\to I}; \Delta\tau) = \nu_Q Q\Delta\tau, \qquad P(E_{Q\to R}; \Delta\tau) = (\gamma_Q + \delta_Q)Q\Delta\tau.$$

$\Delta\tau$ is taken to be small enough that $\sum P(E_\xi;\Delta\tau) \le 1$ for all $\tau \le T$, where $\xi \in \{S \to E, SSE, E \to A, A \to R, E \to I, I \to H, I \to Q, I \to R, H \to I, H \to R, Q \to I, Q \to R\}$ and $T \in \mathbb{R}^+$; this ensures that the above are valid probabilities. We denote the set of all possible transitions as $\mathbb{S}_T$. The stochastic instantaneous rates at which events occur are obtained by dividing the above probabilities by $\Delta\tau$ and taking

$$\lim_{\Delta\tau\to 0^+} \frac{P(E_\xi;\Delta\tau)}{\Delta\tau}$$

for each ξ:

$$\begin{aligned}
q(E_{S\to E}) &= \beta(\eta_A A + I + \eta_Q Q + \eta_H H), & q(E_{SSE}) &= \psi(\eta_A A + I),\\
q(E_{E\to A}) &= q\sigma E, & q(E_{A\to R}) &= (\gamma_A + \delta_A)A,\\
q(E_{E\to I}) &= (1-q)\sigma E, & q(E_{I\to H}) &= \omega_H I,\\
q(E_{I\to Q}) &= \omega_Q I, & q(E_{I\to R}) &= (\gamma_I + \delta_I)I,\\
q(E_{H\to I}) &= \nu_H H, & q(E_{H\to R}) &= (\gamma_H + \delta_H)H,\\
q(E_{Q\to I}) &= \nu_Q Q, & q(E_{Q\to R}) &= (\gamma_Q + \delta_Q)Q.
\end{aligned}$$

From the stochastic instantaneous rates, we obtain the probabilities of given events being the next to occur. Letting $\Omega \doteq \sum q(E_\xi)$, we have:

$$\begin{aligned}
P(E_{S\to E}) &= \frac{q(E_{S\to E})}{\Omega}, & P(E_{SSE}) &= \frac{q(E_{SSE})}{\Omega},\\
P(E_{E\to A}) &= \frac{q(E_{E\to A})}{\Omega}, & P(E_{A\to R}) &= \frac{q(E_{A\to R})}{\Omega},\\
P(E_{E\to I}) &= \frac{q(E_{E\to I})}{\Omega}, & P(E_{I\to H}) &= \frac{q(E_{I\to H})}{\Omega},\\
P(E_{I\to Q}) &= \frac{q(E_{I\to Q})}{\Omega}, & P(E_{I\to R}) &= \frac{q(E_{I\to R})}{\Omega},\\
P(E_{H\to I}) &= \frac{q(E_{H\to I})}{\Omega}, & P(E_{H\to R}) &= \frac{q(E_{H\to R})}{\Omega},\\
P(E_{Q\to I}) &= \frac{q(E_{Q\to I})}{\Omega}, & P(E_{Q\to R}) &= \frac{q(E_{Q\to R})}{\Omega}.
\end{aligned}$$

The set of events $\mathbb{S}_E \doteq \{E_\xi : \xi \in \mathbb{S}_T\}$ and probabilities $\mathbb{S}_P \doteq \{P(E_\xi) : \xi \in \mathbb{S}_T\}$ constitute a continuous-time Markov chain. Our CTMC derivation from the baseline COVID-19 model (1) is adapted from Oluwatobilloba's CTMC derivations from simpler (SIS and SIR) models for infectious disease spread (Oluwatobilloba, 2020). For further reading on infectious disease modeling, see Keeling and Rohani (2008), and for general reading on Markov chains, see Bar-Ilan University (2018) and Queen's University (2005).

2.3. Constancy condition

To investigate the relative influence of SSEs versus non-SSEs on outbreak dynamics, we impose a constancy condition by requiring that the expected number of infections following the first change in state remain constant for different rates of SSEs and non-SSEs. We denote this expectation as $\mathbb{E}_0(X)$, where $X \in \mathbb{N} \cup \{0\}$ is a random variable corresponding to the number of infections following a change in state. Note that these infections may be SSE- or non-SSE-related. Our constancy condition is adapted from James et al.'s (2007) constancy condition. Assuming that James, et al. take $I_0 = 1$, both conditions may be derived using the probability generating functions (pgfs) of X given the systems' initial states. However, the interpretation of $E_0(X)$ differs, as the systems' state changes have different meanings (see Section 2.5).

Let $\beta^* = \kappa\beta$, where $\kappa \in [0,1]$ and β is the fitted infection rate parameter (see Table 1), which we take to be the non-SSE rate in the absence of SSEs. This gives $\beta^* \in [0,\beta]$. We seek ψ, the SSE rate, such that the constancy condition is satisfied for an arbitrary β^*. To begin, we derive the pgf for X. Letting

$$\begin{aligned}
\tilde{P}(X=0) = {} & P(E_{EA}) + P(E_{AR}) + P(E_{EI}) + P(E_{IH}) + P(E_{IQ})\\
& + P(E_{IR}) + P(E_{HI})\\
& + P(E_{HR}) + P(E_{QI}) + P(E_{QR})
\end{aligned}$$

and recalling that $K \sim \text{Poisson}(\phi)$, we have:

$$\begin{aligned}
G(s) &= P(X=0)s^0 + P(X=1)s^1\\
&\quad + P(X=2)s^2 + \cdots + P(X=k)s^k + \cdots\\
&= [P(E_{SSE}\ \&\ K=0) + \tilde{P}(X=0)]s^0\\
&\quad + [P(E_{SSE}\ \&\ K=1) + P(E_{SE})]s^1\\
&\quad + P(E_{SSE}\ \&\ K=2)s^2 + \ldots + P(E_{SSE}\ \&\ K=k)s^k + \cdots\\
&= \tilde{P}(X=0)s^0 + P(E_{SE})s^1 + P(E_{SSE})[P(K=0)s^0 + P(K=1)s^1\\
&\quad + P(K=k)s^k + \cdots]\\
&= \tilde{P}(X=0)s^0 + P(E_{SE})s^1 + P(E_{SSE})[\tfrac{\phi^0}{0!}e^{-\phi}s^0 + \tfrac{\phi^1}{1!}e^{-\phi}s^1\\
&\quad + \tfrac{\phi^2}{2!}e^{-\phi}s^2 +\\
&\quad \ldots + \tfrac{\phi^k}{k!}e^{-\phi}s^k + \cdots]\\
&= \tilde{P}(X=0) + P(E_{SE})s + P(E_{SSE})e^{\phi(s-1)}
\end{aligned}$$

From the pgf, we obtain the expectation of X:

$$\begin{aligned}
\mathbb{E}(X) &= G'(1) = P(E_{SE}) + P(E_{SSE})\phi\\
&= \frac{\beta(\eta_A A + I + \eta_H H + \eta_Q Q) + \psi(\eta_A A + I)\phi}{\Omega}
\end{aligned}$$

Taking $\langle E, A, I, H, Q\rangle = \langle E_0, A_0, I_0, H_0, Q_0\rangle$, where the latter are the initial numbers of exposed, asymptomatic, symptomatic, hospitalized, and quarantined individuals, $\mathbb{E}(X)$ becomes $\mathbb{E}_0(X)$. For further reading on pgfs and their properties and epidemiological applications, see Miller (2018) and University of Cambridge (2008).

Next, we obtain ψ as a function of β^*. Letting $\mathbb{E}_{0,\beta}(X)$ and $\mathbb{E}_{0,\beta^*}(X)$ be the initial expectations when the non-SSE rates are β and $\beta^* < \beta$ and setting $E_{0,\beta}(X) = E_{0,\beta^*}(X)$, we have:

$$\begin{aligned}
\psi = \frac{I_1(\beta-\beta^*)\Omega'}{I_2[\phi\Omega' + \beta I_1(\phi-1)]}, \quad I_1 &= \eta_A A_0 + I_0 + \eta_H H_0 + \eta_Q Q_0\\
I_2 &= \eta_A A_0 + I_0\\
\Omega' &= \sigma E_0 + (\gamma_A + \delta_A)A_0\\
&\quad + (\omega_H + \omega_Q + \gamma_I + \delta_I)I_0\\
&\quad + (\nu_H + \gamma_H + \delta_H)H_0\\
&\quad + (\nu_Q + \gamma_Q + \delta_Q)Q_0
\end{aligned} \tag{2}$$

Note that ψ is only defined for $I_2, \phi\Omega' + \beta I_1(\phi-1) > 0$. The requirement that ψ be of the above form constitutes our constancy condition.

Also note that ψ is invariant under scaling with respect to $\langle E_0, A_0, I_0, H_0, Q_0\rangle$. Indeed, letting $c \in \mathbb{R}$, $\vec{v} = \langle E_0, A_0, I_0, H_0, Q_0\rangle$, and $\vec{w} = \langle \sigma, \eta_A, \eta_H, \eta_Q, \omega_H, \omega_Q, \nu_H, \nu_Q, \gamma_A, \gamma_I, \gamma_H, \gamma_Q, \delta_A, \delta_I, \delta_H, \delta_Q\rangle$ and noting that $I_1(c\vec{v};\vec{w}) = cI_1(\vec{v};\vec{w})$, $I_2(c\vec{v};\vec{w}) = cI_2(\vec{v};\vec{w})$, and $\Omega'(c\vec{v};\vec{w}) = c\Omega'(\vec{v};\vec{w})$, we have:

$$\begin{aligned}
\psi(c\vec{v};\vec{w}) &= \frac{I_1(c\vec{v};\vec{w})(\beta-\beta^*)\Omega'(c\vec{v};\vec{w})}{I_2(c\vec{v};\vec{w})[\phi\Omega'(c\vec{v};\vec{w}) + \beta I_1(c\vec{v};\vec{w})(\phi-1)]}\\
&= \frac{cI_1(\vec{v};\vec{w})(\beta-\beta^*)c\Omega'(\vec{v};\vec{w})}{cI_2(\vec{v};\vec{w})[\phi c\Omega'(\vec{v};\vec{w}) + \beta cI_1(\vec{v};\vec{w})(\phi-1)]}\\
&= \frac{I_1(\vec{v};\vec{w})(\beta-\beta^*)\Omega'(\vec{v};\vec{w})}{I_2(\vec{v};\vec{w})[\phi\Omega'(\vec{v};\vec{w}) + \beta I_1(\vec{v};\vec{w})(\phi-1)]}\\
&= \psi(\vec{v};\vec{w})
\end{aligned}$$

This property motivates our choice of initial conditions when simulating the CTMC model (see Section 2.4).

2.4. Model simulation

Because our model is a CTMC, it may be simulated using Gillespie's direct algorithm (Keeling and Rohani, 2008; Gillespie, 1976). The algorithm is a direct (versus approximate; see Wilasang et al. (2022)) method for simulating stochastic processes (Gillespie, 1976). We simulated the model under the following scenarios:

(i). Neither hospitalization nor quarantine (NHQ), in which hospitalization, quarantine, premature hospital discharge, and quarantine violation are excluded from the model; this is equivalent to excluding $E_{I\to H}$, $E_{I\to Q}$, $E_{H\to I}$, and $E_{Q\to I}$ from the model

(ii). Realistic hospitalization and quarantine (RHQ), in which hospitalization, quarantine, premature hospital discharge, and quarantine violation are included in the model; this is equivalent to including $E_{I\to H}$, $E_{I\to Q}$, $E_{H\to I}$, and $E_{Q\to I}$ in the model

(iii). Idealistic hospitalization and quarantine (IHQ), in which hospitalization and quarantine are included in the model but premature hospital discharge and quarantine violation are excluded; this is equivalent to including $E_{I\to H}$ and $E_{I\to Q}$ in the model but excluding $E_{H\to I}$ and $E_{Q\to I}$

Note that RHQ corresponds to the baseline COVID-19 model (1). We also simulated the model under RHQ with low quarantine violation (*lqv*) and high quarantine violation (*hqv*). We denote these sub-scenarios as RHQ_{lqv} and RHQ_{hqv}. For *lqv*, we halved the fitted value of quarantine violation ($\frac{1}{2}\nu_Q$), and for *hqv*, we doubled the fitted value of quarantine violation ($2\nu_Q$).

Events were excluded by setting their corresponding stochastic instantaneous rates to zero. In NHQ, ω_H, ω_Q, ν_H, and ν_Q were set to zero, thereby eliminating hospitalization, quarantine, premature hospital discharge, and quarantine violation; in RHQ, ω_H, ω_Q, ν_H, and ν_Q remained set to their fitted values (see Table 1); and in IHQ, ω_H and ω_Q remained set to their fitted values, while ν_H and ν_Q were set to zero, thereby eliminating premature hospital discharge and quarantine violation.

The initial conditions for NHQ, RHQ, and IHQ were $\langle E_0, A_0, I_0, H_0, Q_0\rangle = \langle 15, 2, 4, 0, 0\rangle$, $\langle 14, 2, 2, 1, 1\rangle$, and $\langle 14, 2, 2, 1, 1\rangle$, respectively; the CTMC model is independent of S_0 and R_0. These initial conditions were obtained by simulating the baseline COVID-19 model (1) under each scenario with $\langle S_0, E_0, A_0, I_0, H_0, Q_0, R_0\rangle = \langle 10^{10}, 20, 0, 0, 0, 0, 0\rangle$ and recording the number of individuals in each class on day 3. S_0 was taken to be 10^{10} to ensure that the depletion of susceptible individuals had a negligible influence. Recall that the constancy condition is not defined for $\langle E_0, A_0, I_0, H_0, Q_0\rangle = \vec{0}$ and is invariant under scaling of $\langle E_0, A_0, I_0, H_0, Q_0\rangle$ (see Section 2.3). This motivates the need for a realistic initial proportion of asymptomatic, symptomatic, hospitalized, and quarantined individuals. The initial conditions for RHQ_{lqv} and RHQ_{lqv} were taken to be the same as for RHQ.

For NHQ, RHQ, and IHQ, κ was varied from 0 to 1 in increments of 0.1, and ψ was calculated for each β^* value using the constancy condition (Eq. (2)) with scenarios' corresponding initial conditions and parameter sets. κ was also varied from 0 to 1 in increments of 0.1 for RHQ_{lqv} and RHQ_{hqv}, but ψ was taken to be the same as for RHQ; it was not re-calculated using $\frac{1}{2}\nu_Q$ or $2\nu_Q$. This allows for better isolation of quarantine violation's influence on quarantine effectiveness for SSE- versus non-SSE-dominated outbreaks.

Simulations were ended once either the disease went extinct or 50 active infections were attained, similar to the approach taken in Lloyd-Smith et al. (2005). The number of extinctions and total simulations were recorded to estimate the probabilities of outbreak extinction, and for surviving outbreaks, the times at which 50 active infections were attained and the cumulative numbers of SSE-related and non-SSE-related infections were recorded for analysis; these times are hereafter referred to as stop times. The total simulations is the combined number of extinction simulations, defined here as simulations in which the disease went extinct before attaining 50 active infections, and non-extinction simulations. Note that there are other non-extinction metrics, such as the pathogen circulating in the population for a long period of time (Thompson et al., 2020).

The number of non-extinction simulations depended on the variances of the stop times; additional simulations were ran until the desired number of non-extinction simulations were completed. If the variance was less than 1500, 50 000 non-extinction simulations were completed; if the variance was between 1500 and 15 000, 500 000 non-extinction simulations were completed; and if the variance was greater than 15 000, 1 500 000 non-extinction simulations were completed.

Table 2
Number of non-extinction simulations completed for each parameter set. $\langle 0, 0, 0, 0\rangle$ corresponds to NHQ, $\langle 0.453, 0.1977, 0.23025, 0.1301\rangle$ corresponds to RHQ_{lqv}, $\langle 0.453, 0.1977, 0.4605, 0.1301\rangle$ corresponds to RHQ, $\langle 0.453, 0.1977, 0.921, 0.1301\rangle$ corresponds to RHQ_{hqv}, and $\langle 0.453, 0.1977, 0, 0\rangle$ corresponds to IHQ.

$\langle\omega_Q, \omega_H, \nu_Q, \nu_H\rangle$	κ	Non-extinction simulations
$\langle 0, 0, 0, 0\rangle$	[0, 1]	50 000
$\langle 0.453, 0.1977, 0.23025, 0.1301\rangle$	[0, 0.6]	500 000
$\langle 0.453, 0.1977, 0.23025, 0.1301\rangle$	[0.7, 1]	50 000
$\langle 0.453, 0.1977, 0.4605, 0.1301\rangle$	[0, 0.4]	500 000
$\langle 0.453, 0.1977, 0.4605, 0.1301\rangle$	[0.5, 1]	50 000
$\langle 0.453, 0.1977, 0.921, 0.1301\rangle$	[0, 1]	50 000
$\langle 0.453, 0.1977, 0, 0\rangle$	[0, 0.3]	50 000
$\langle 0.453, 0.1977, 0, 0\rangle$	[0.4, 0.5]	500 000
$\langle 0.453, 0.1977, 0, 0\rangle$	[0.6, 0.8]	1 500 000
$\langle 0.453, 0.1977, 0, 0\rangle$	[0.9, 1]	500 000

Table 2 gives the number of non-extinction simulations completed for each parameter set.

2.5. Discrete-time Markov chain models

With CTMC models, the system may assume a new state at any time $t \in \mathbb{R}^+$; t is thus continuous. For our CTMC model, every time-step corresponds to a single event E_ξ, $\xi \in \mathbb{S}_T$, occurring. With discrete-time Markov chain (DTMC) models, the system may only assume a new state at times $\{t_k : k \in \mathbb{N}\}$; t is thus discrete. For Lloyd-Smith et al.'s (2005) and James et al.'s (2007) DTMC models, every time-step corresponds to the death of the current generation of infected individuals and birth of the next generation of infected individuals. The CTMC and DTMC models' state changes thus have different meanings.

Lloyd-Smith et al. (2005) utilize an individual-based superspreading framework. They incorporate superspreading individuals into their DTMC via the random variable ν, the expected number of infections caused by an individual. Individuals thus have different potentials to infect others. They simulate their model under multiple scenarios, each of which assumes a different distribution for ν. We limit our comparison (see Section 4) to the scenario which assumes ν is γ-distributed. James et al. (2007) utilize an event-based framework. They incorporate SSEs into their DTMC via ρ, the expected number of SSEs caused by an individual, and λ, the expected number of infections caused by an SSE. Every individual has the same potential to infect others.

3. Results

The results are divided by scenario, and the goals (see Section 1) addressed by each scenario are indicated in their respective sections. Note that G1 is addressed by all scenarios, while G2 and G3 are addressed by only some scenarios. In each figure, κ increases from 0 to 1 in increments of 0.1; increasing values of κ correspond to decreasing rates of SSEs and increasing rates of non-SSEs. Note that, while all figures' x-axes are the same, their y-axes differ. A table containing the margins of error for the means of stop times' 95% confidence intervals is given in Appendix A (see Table 3).

Scenario (i): Neither hospitalization nor quarantine (NHQ)

NHQ addresses G1 and G2. In this scenario, hospitalization, quarantine, premature hospital discharge, and quarantine violation are excluded from the model. Fig. 2(a) shows the distribution of stop times. The maximum, mean, and median stop times strictly decrease for $\kappa \in [0, 1]$, while the minimum stop times are similar for $\kappa \in [0, 0.7)$ but strictly increase for $\kappa \in [0.7, 1]$. Figs. 2(b) and 2(c) show the variances of stop times and probabilities of extinction, respectively. Both strictly decrease for $\kappa \in [0, 1]$, but they do so more quickly for smaller κ. Fig. 2(d) shows the means of the cumulative numbers of SSE-related and non-SSE-related infections. The SSE curve strictly decreases with

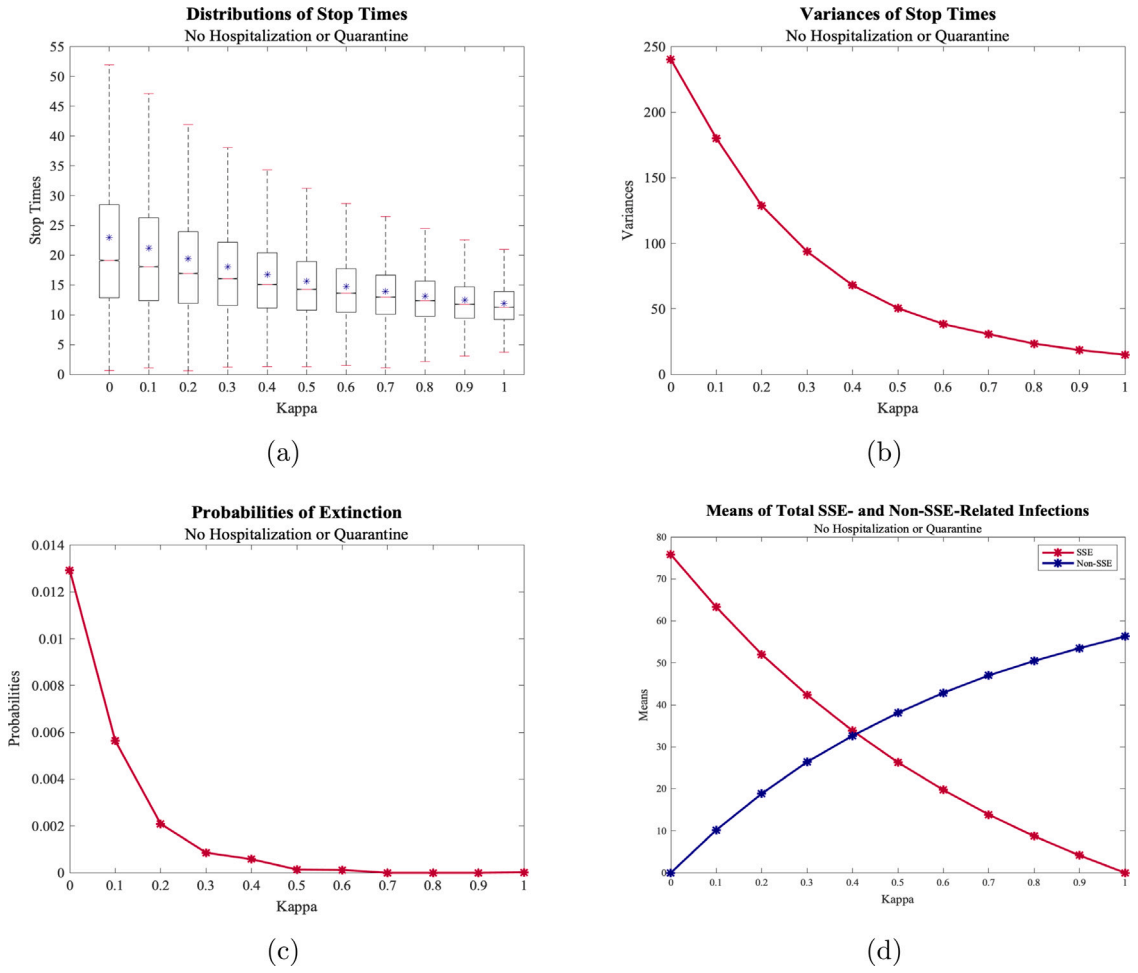

Fig. 2. (a) Distributions of stops times (NHQ) (b) Variances of stop times for NHQ (c) Probabilities of extinction for NHQ (d) Means of cumulative total of SSE- and non-SSE-related infections for NHQ; their curves are labeled as SSE and non-SSE.

increasing κ, while the Non-SSE curve strictly increases. They do so more quickly for smaller κ and intersect between $\kappa = 0.4$ and $\kappa = 0.5$.

Scenario (ii): Realistic hospitalization and quarantine (RHQ)

RHQ also addresses G1 and G2. In this scenario, hospitalization, quarantine, premature hospital discharge, and quarantine violation are included in the model. Fig. 3(a) shows the distribution of stop times. The maximum, mean, and median stop times strictly decrease for $\kappa \in [0, 1]$, while the minimum stop times are similar for $\kappa \in [0, 0.5)$ but generally increase for $\kappa \in [0.5, 1]$. Figs. 3(b) and 3(c) show the variances of stop times and probabilities of extinction, respectively. Both strictly decrease for $\kappa \in [0, 1]$, but they do so more quickly for smaller κ, the exception being the variances of stop times for $\kappa \in [0, 0.1]$. Fig. 3(d) shows the means of the cumulative numbers of SSE-related and non-SSE-related infections. The SSE curve strictly decreases with increasing κ, while the Non-SSE curve strictly increases. They do so more quickly for smaller κ and intersect between $\kappa = 0.4$ and $\kappa = 0.5$.

Scenario (iii): Idealistic quarantine and hospitalization (IHQ)

IHQ also addresses G1 and G2. In this scenario, hospitalization and quarantine are included in the model, but premature hospital discharge and quarantine violation are excluded. Fig. 4(a) shows the distribution of stop times. The maximum, mean, and median stop times strictly increase for $\kappa \in [0, 0.7)$ but strictly decrease for $\kappa \in [0.7, 1]$. Meanwhile, the minimum stop times are similar for $\kappa \in [0, 0.8)$ but strictly increase for $\kappa \in [0.8, 1]$. Fig. 4(b) shows the variances of stop times, which strictly increase for $\kappa \in [0, 0.7)$ but strictly decrease for $\kappa \in [0.7, 1]$. Fig. 4(c) shows the probabilities of extinction, which strictly decrease with increasing κ for $\kappa \in [0, 1]$ but remain near 1 for $\kappa \in [0, 0.5)$ and quickly decrease for $\kappa \in [0.5, 1]$. Fig. 4(d) shows the means of the cumulative numbers of SSE-related and non-SSE-related infections. The SSE curve remains approximately constant for $\kappa \in [0, 0.5)$ but strictly decreases for $\kappa \in [0.5, 1]$. Meanwhile, the Non-SSE curve strictly increases for $\kappa \in [0, 0.7)$, remains approximately constant for $\kappa \in [0.7, 0.8)$, and strictly decreases for $\kappa \in [0.8, 1]$. The curves intersect between $\kappa = 0.4$ and $\kappa = 0.5$.

Varying quarantine violation

RHQ_{lqv} and RHQ_{hqv} address G1 and G3. In RHQ_{lqv}, RHQ's quarantine violation level is halved, and in RHQ_{hqv}, RHQ's quarantine violation level is doubled. Figs. 5(a), 5(b), 5(c), and 5(d) contain curves for RHQ_{lqv}, RHQ, and RHQ_{hqv}. Figs. 5(a) and 5(b) show the means and variances of stop times for each quarantine violation level. For RHQ_{lqv}, both strictly increase for $\kappa \in [0, 0.2)$ but strictly decrease for $\kappa \in [0.2, 1]$; for RHQ and RHQ_{hqv}, both strictly increase for $\kappa \in [0, 1]$. The means and variances of stop times strictly decrease going from RHQ_{lqv} to RHQ to RHQ_{hqv} for each $\kappa \in [0, 1]$, but their differences are greater for smaller κ. Fig. 5(c) shows the probabilities of extinction. They strictly decrease for $\kappa \in [0, 1]$ but do so more quickly for smaller κ. The probabilities of extinction also strictly decrease going from RHQ_{lqv} to RHQ to RHQ_{hqv} for $\kappa \in [0, 1]$, but their differences are greater for smaller κ. They decrease more quickly for RHQ_{lqv} than RHQ and RHQ_{hqv}. Fig. 5(d) shows the cumulative numbers of SSE-related

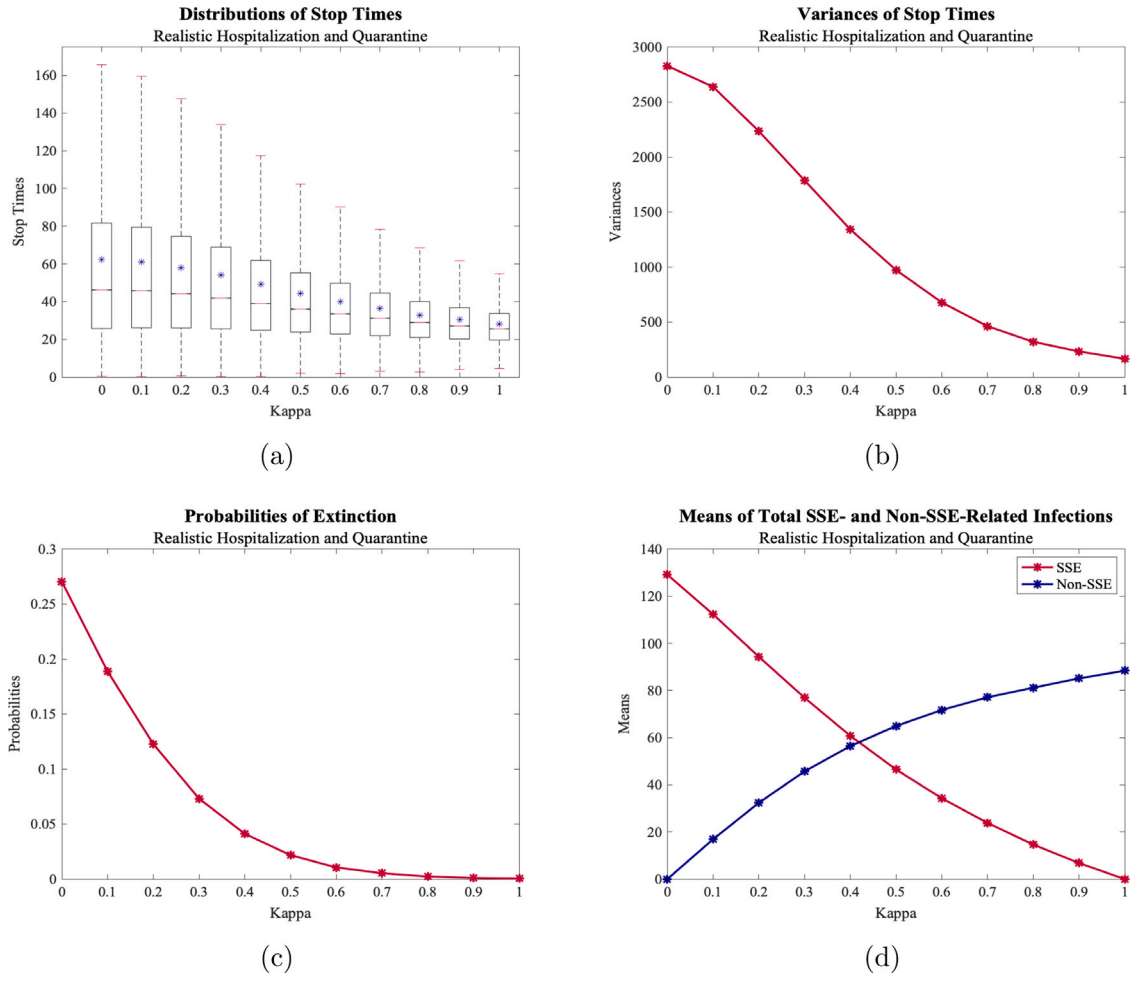

Fig. 3. (a) Distributions of stops times (RHQ) (b) Variances of stop times for RHQ (c) Probabilities of extinction for RHQ (d) Means of cumulative total of SSE- and non-SSE-related infections for RHQ; their curves are labeled as SSE and non-SSE.

infections. They strictly decrease for $\kappa \in [0,1]$ but do so more quickly for smaller κ, the exception being RHQ_{lqv} for $\kappa \in [0,0.2)$.

4. Discussion

The discussion is divided into three subsections. In the first subsection, we discuss results from simulating the CTMC model under the main scenarios (NHQ, RHQ, and IHQ); recall that this allows us to investigate the effectiveness of hospitalization and quarantine as control measures for SSE versus non-SSE-dominated outbreaks (G2). In the second subsection, we discuss results from varying quarantine violation (RHQ_{lqv} and RHQ_{hqv}); recall that this allows us to investigate the influence of quarantine violation on the effectiveness of quarantine for SSE- versus non-SSE-dominated outbreaks (G3). In both of the aforementioned subsections, we discuss the results from varying SSE and non-SSE rates, as this is done in all scenarios; recall that this allows us to investigate the influence of SSEs relative to that of non-SSEs on outbreak dynamics (G1). Further recall that varying SSE and non-SSE rates is accomplished by varying κ; as κ increases, non-SSE rates increase, and SSE rates decrease. If $\kappa = 0.X$, $X \in \{1,2,3,4,5,6,7,8,9\}$, then the non-SSE rate is $X0\%$ of its fitted value (Table 1); for example, if $\kappa = 0.5$, then the non-SSE rate is 50% of its fitted value. When the non-SSE rate is decreased from its fitted value, the SSE rate is increased according to the constancy condition (see Section 2). In the third subsection, we compare our results to those of other superspreading models in literature.

Simulating the model under the main scenarios

For both NHQ and RHQ, most outbreaks are more variable but less severe when SSE rates are higher, as evidenced by the variances of stop times in Figs. 2(b) and 3(b) and the distributions of stop times in Figs. 2(a) and 3(a). Here, severity is based on stop times; more severe outbreaks are quicker to attain 50 active infections, while less severe outbreaks are slower. Though most SSE-dominated outbreaks are less severe, the most severe SSE-dominated outbreaks are more severe than the most severe non-SSE-dominated outbreaks, as evidenced by the minimum stop times in Figs. 2(a) and 3(a). While the differences in minimum stop times are small, they are significant in practice because the minimum stop times themselves are small; when there are few days to formulate a public health response, every additional day helps. For example, if there is only 3 days to respond, an additional 2 days may make a difference. Outbreaks are also more likely to go extinct when SSE rates are higher, as evidenced by the probabilities of extinction in 2(c) and 3(c). All of the aforementioned observations hold for IHQ when $\kappa \in [0.7,1]$ but not when $\kappa \in [0,0.7)$. For IHQ when $\kappa \in [0,0.7)$, most outbreaks are less variable (see Fig. 4(b)) but more severe (see Fig. 4(a)) when SSE rates are higher. The most severe SSE-dominated outbreaks are still more severe than the most severe non-SSE-dominated outbreaks (see Fig. 4(a)), and outbreaks are still more likely to go extinct (see Fig. 4(c)) when SSE rates are higher. Going from NHQ ($\kappa \in [0,1]$) to RHQ ($\kappa \in [0,1]$) to IHQ ($\kappa \in [0.7,1]$), outbreaks increase in variability (see Figs. 2(b), 3(b), and 4(b)), decrease in severity (see Figs. 2(a), 3(a), and 4(a)), and are more

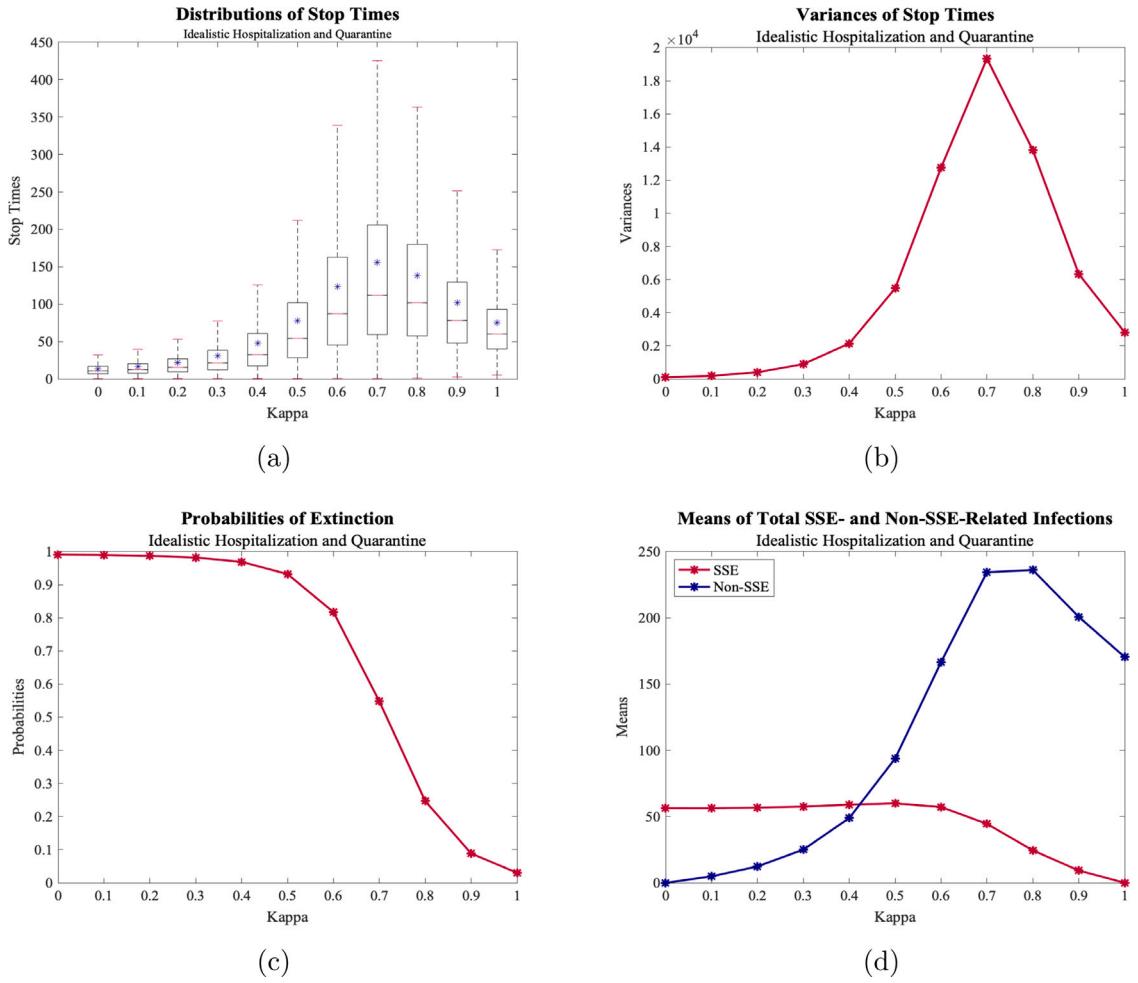

Fig. 4. (a) Distributions of stops times (b) Variances of stop times for IHQ (c) Probabilities of extinction for IHQ (d) Means of cumulative total of SSE- and non-SSE-related infections for IHQ; their curves are labeled as SSE and non-SSE.

likely to go extinct (see Figs. 2(c), 3(c), and 4(c)). Figures showing the variances of stop times and probabilities of extinction across scenarios are given in Appendix B (see Figs. 6(a) and 6(b)).

Differences for IHQ when $\kappa \in [0, 0.7)$ are likely related to high probabilities of extinction. For $\kappa \in [0, 0.7)$, outbreaks may be less variable but more severe when SSE rates are higher because surviving outbreaks are restricted to those with many SSE-related infections early on. This is evidenced by the means of cumulative SSE-related infections remaining approximately constant when $\kappa \in [0, 0.5)$ despite decreasing SSE rates, after which they decrease with decreasing SSE rates, as expected (see Fig. 4(d)). Meanwhile, the means of total non-SSE-related infections increase with increasing non-SSE rates when $\kappa \in [0, 0.7)$, as expected, but decrease when $\kappa \in [0.7, 1]$ despite increasing non-SSE rates (see Fig. 4(d)). The weakening pull towards extinction may allow 50 active infections to be attained more quickly (see Fig. 4(a)), to the extent that the number of cumulative infections is reduced. For NQH and RHQ, the probabilities of extinction are lower than for IHQ (see Figs. 2(c), 3(c), and 4(c)), and the means of cumulative SSE-related and non-SSE-related infections for NHQ and RHQ decrease with decreasing SSE rates and increase with increasing non-SSE rates (see Figs. 2(d) and 3(d)), as expected. A figure showing the means of cumulative SSE-related infections across scenarios is given in Appendix B (see Fig. 6(c)). Note that for NHQ and RHQ, the means of cumulative SSE-related infections decrease more quickly for smaller κ (see Figs. 2(d) and 3(d)), while for IHQ, the means of cumulative SSE-related infections decrease more slowly for smaller κ when $\kappa \in [0.5, 0.7)$ but more quickly for smaller κ when $\kappa \in [0.7, 1]$ (see Fig. 4(d)). This, in conjunction with the slight lag between the means of cumulative SSE-related infections decreasing and outbreaks becoming more variable but less severe when SSE rates are higher, suggests that $\kappa \in [0.5, 0.7)$ corresponds to a transitional period. During this period, dynamics change from those only observed for IHQ to those also observed for NHQ and RHQ.

Greater variability in SSE-dominated outbreaks may limit predictions. Increased variability increases prediction uncertainty, which may decrease prediction accuracy. Increased prediction uncertainty also shortens the time period over which predictions hold. Such limitations impede public health responses. Meanwhile, taking more time in most cases to attain 50 active infections when SSE rates are higher may allow the virus to avoid detection for longer; more sensitive and stable surveillance systems are necessary to detect the virus at low levels. Because even slow SSE-dominated outbreaks may abruptly take off, timeliness is also key. For further information on the stability, sensitivity, and timeliness of surveillance systems, see Centers for Disease Control and Prevention (2001) and Centers for Disease Control and Prevention (2021b). Persistence at low levels also facilitates the evolution of more infectious variants (Antia et al., 2003; Woolhouse et al., 2005). The public health consequences associated with SSE-dominated outbreaks are, in some cases, mitigated by high probabilities of extinction. For IHQ, SSE-dominated outbreaks almost always go extinct; for RHQ, SSE-dominated outbreaks are somewhat likely to go extinct. Public health consequences are thus mostly mitigated for IHQ and somewhat mitigated for RHQ. They are not, however, mitigated for NHQ, as outbreaks (SSE- or non-SSE-dominated) seldom go extinct in this scenario. SSE-dominated outbreaks almost always go extinct for

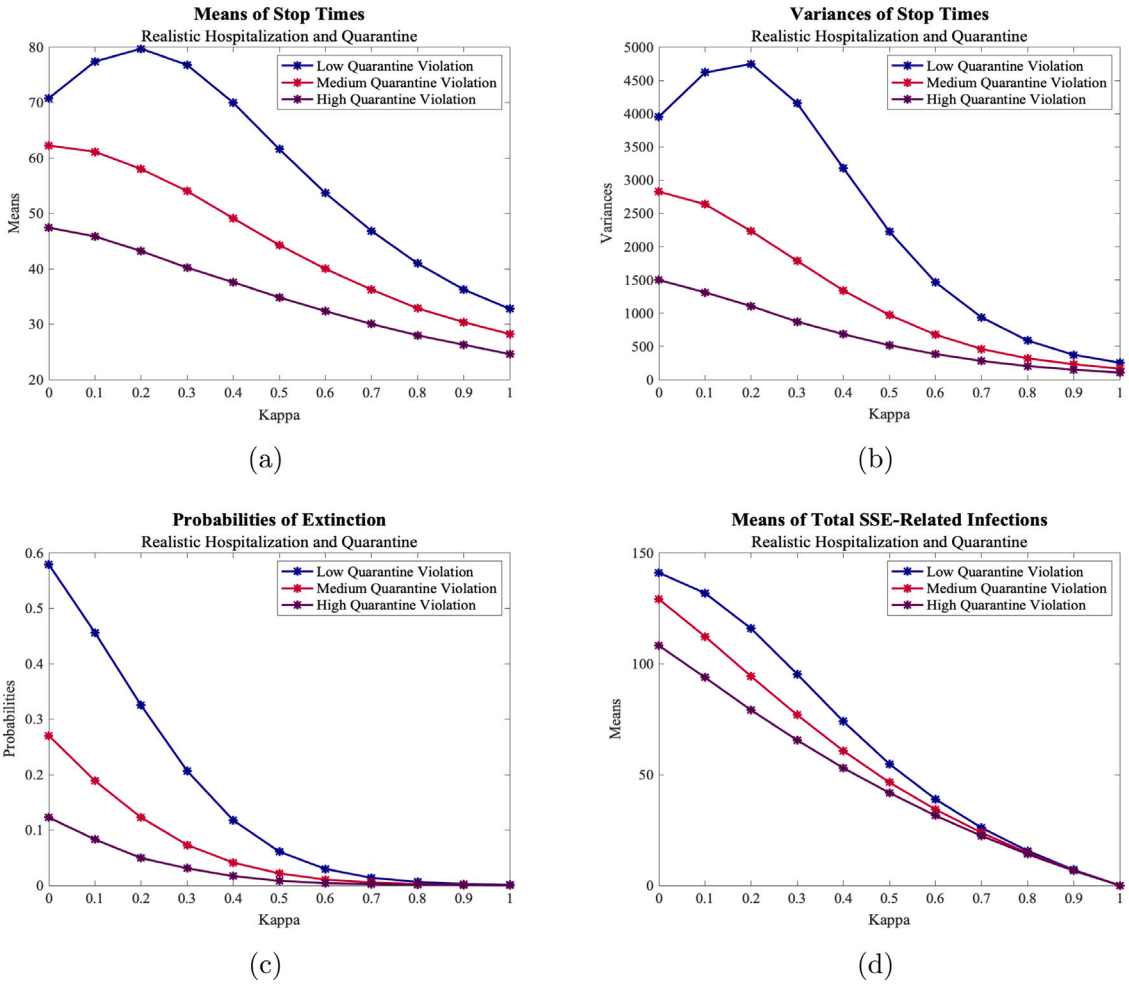

Fig. 5. (a) Means of stops times for RHQ_{lqv}, RHQ, and RHQ_{hqv} (b) Variances of stop times for RHQ_{lqv}, RHQ, and RHQ_{hqv} (c) Probabilities of extinction for RHQ_{lqv}, RHQ, and RHQ_{hqv} (d) Means of cumulative total of SSE-related infections for RHQ_{lqv}, RHQ, and RHQ_{hqv}. Curves for RHQ_{lqv}, RHQ, and RHQ_{hqv} are labeled as low quarantine violation, medium quarantine violation, and high quarantine violation.

IHQ because we assume that neither hospitalized (H) nor quarantined (Q) individuals cause SSEs, and control measures significantly reduce the number of symptomatic (I) individuals available to cause SSEs in IHQ; recall that in IHQ, there is perfect control, while in NHQ and RHQ, there is no control and imperfect control, respectively. This implies that, in general, when those capable of causing SSEs are targeted with perfect control, SSE-dominated outbreaks almost always go extinct.

Across the board decreases in probabilities of extinction going from IHQ to RHQ to NHQ suggest that including hospitalization and quarantine and decreasing premature hospital discharge and quarantine violation forces more outbreaks to extinction. Greater differences for SSE-dominated outbreaks versus non-SSE-dominated outbreaks imply that hospitalization and quarantine are more effective at controlling SSE-dominated outbreaks; likewise, premature hospital discharge and quarantine violation are more consequential for such outbreaks. Quicker decreases in probabilities of extinction for IHQ, RHQ, and NHQ when SSE rates are higher further imply that SSE-dominated outbreaks are more sensitive to changes in hospitalization, quarantine, premature hospital discharge, and quarantine violation. High probabilities of extinction for IHQ when SSE rates are higher, in conjunction with the quicker decreases, imply that reducing premature hospital discharge and quarantine violation substantially increases the effectiveness of hospitalization and quarantine at forcing SSE-dominated outbreaks to extinction. Altogether, these results highlight the importance of implementing control measures and limiting factors that reduce control measure effectiveness in SSE-dominated outbreaks; doing so increases the probability of extinction from ≈ 0 to ≈ 1 for $\kappa \leq 0.4$ (see Figs. 2(c), 3(c), and 4(c)). When weighing the benefits and detriments of control measures, the relative rates of SSEs versus non-SSEs should be considered; for more on the benefits and detriments of control measures, see Jamison et al. (2018, Chapter 17). Note that in all of the aforementioned, the effectiveness of hospitalization and quarantine and the consequences of premature hospital discharge and quarantine violation were evaluated using probabilities of extinction versus other metrics, such as cumulative infections or deaths; the latter metrics would be misleading because simulations were ended once either the disease went extinct or 50 active infections were attained (see Section 2).

Varying quarantine violation

For RHQ_{lqv}, outbreaks are more variable but less severe on average when SSE rates are higher (see Figs. 5(b) and 5(a)), similar to NHQ and RHQ; for RHQ_{hqv}, outbreaks are less variable but more severe on average for $\kappa \in [0, 0.2)$ and more variable but less severe on average for $\kappa \in [0.2, 1]$ when SSE rates are higher (see Figs. 5(b) and 5(a)), similar to IHQ. For RHQ_{lqv} and RHQ_{hqv}, outbreaks are more likely to go extinct when SSE rates are higher (see Fig. 5(c)), similar to NHQ, RHQ, and IHQ. The means of total SSE-related infections decrease with decreasing SSE rates for RHQ_{lqv}, RHQ, and RHQ_{hqv}, but they do so more slowly for RHQ_{lqv} than RHQ or RHQ_{hqv} when SSE rates are higher (see Fig. 5(d)). We expect the opposite, given that quarantined individuals cannot cause SSEs. Going from RHQ to RHQ_{hqv}, the means of total SSE-related

infections decrease more slowly, as expected. Differences for RHQ_{lqv} when $\kappa \in [0, 0.2)$ may thus be related to high probabilities of extinction (see Fig. 5(c)), with $\kappa \in [0, 0.2)$ corresponding to a transitional period, similar to IHQ with $\kappa \in [0.5, 0.7)$.

Going from RHQ_{lqv} ($\kappa \in [0, 1]$) to RHQ ($\kappa \in [0, 1]$) to RHQ_{hqv} ($\kappa \in [0.2, 1]$), outbreaks decrease in variability, increase in severity, and are less likely to go extinct (see Figs. 5(b), 5(a), and 5(c)). These differences are greater for SSE-dominated outbreaks, most notably with respect to variability and extinction. Taking less time on average to attain 50 active infections when quarantine violation is higher shortens the time period during which outbreaks may feasibly be contained; the further outbreaks progress, the harder it becomes to contain them (Maxmen, 2021). While lesser variability in outbreaks when quarantine violation is higher allows for lesser prediction uncertainty, it also allows for a greater number of more severe outbreaks, given that outbreaks are more severe on average when quarantine violation is higher. Larger numbers of infections over shorter time periods may strain resources (Centers for Disease Control and Prevention, 2021a). Across the board increases in probabilities of extinction going from RHQ_{hqv} to RHQ to RHQ_{lqv} suggest that decreasing quarantine violation forces more outbreaks to extinction. Greater differences for SSE-dominated versus non-SSE-dominated outbreaks imply that quarantine violation is more consequential for SSE-dominated outbreaks. Quicker decreases in probabilities of extinction for RHQ_{lqv}, RHQ, and RHQ_{hqv} when SSE rates are higher further imply that SSE-dominated outbreaks are more sensitive to changes in quarantine violation. High probabilities of extinction for RHQ_{lqv} when SSE rates are higher, in conjunction with the quicker decreases, imply that reducing quarantine violation substantially increases the effectiveness of quarantine at forcing SSE-dominated outbreaks to extinction. This reinforces our previous findings regarding premature hospital discharge and quarantine violation. Again note that in all of the aforementioned, the effectiveness of quarantine and consequences of quarantine violation were evaluated using probabilities of extinction versus other metrics, such as cumulative infections or deaths; the latter metrics would be misleading because simulations were ended once either the disease went extinct or 50 active infections were attained (see Section 2).

Comparison with superspreading models in literature

Lloyd-Smith et al. (2005) and James et al. (2007) utilize discrete-time Markov Chain (DTMC) models to investigate the relative influences of SIs and SSEs on outbreak dynamics. Their DTMC models' underlying biological process is more simplistic than ours; susceptible individuals are infected and infected individuals recover. There are neither exposed, asymptomatic, hospitalized, nor quarantined individuals. DTMC models also evolve through time differently, and their state changes have different meanings. For further information on how Lloyd, et al. and James, et al. incorporate SIs and SSEs into their DTMC models, as well as further information on the differences between DTMCs and CTMCs, see Section 2.5.

Lloyd-Smith et al. (2005) and James et al. (2007) found that increasing SIs or SSEs relative to non-SIs or non-SSEs increases the probability that outbreaks go extinct but decreases the variability of surviving outbreaks, which are more severe when dominated by SIs or SSEs. This partially agrees with our findings for NHQ ($\kappa \in [0, 1]$), RHQ ($\kappa \in [0, 1]$), and IHQ ($\kappa \in [0.7, 1]$) – increasing SSEs relative to non-SSEs increases both the probability that outbreaks go extinct and the variability of surviving outbreaks, which are less severe when dominated by SSEs – and fully agrees with our findings for IHQ ($\kappa \in [0, 0.7)$). While the probabilities of extinction increase with increasing influence of SIs or SSEs relative to non-SIs or non-SSEs for Lloyd, et al.'s, James, et al.'s, and our model, they approach different values. For the individual-based model, they approach 1, but for the event-based models, they do not. This suggests that SSE-dominated outbreaks are more likely to survive than SI-dominated outbreaks.

Differences in the variability and severity of surviving outbreaks between Lloyd-Smith et al.'s (2005), James et al.'s (2007), and our model for NQH ($\kappa \in [0, 1]$), RHQ ($\kappa \in [0, 1]$), and IHQ ($\kappa \in [0, 0.7)$) may be related to differences in probabilities of extinction, which are higher for Lloyd-Smith et al.'s (2005), James et al.'s (2007), and our model for IHQ ($\kappa \in [0.7, 1]$). Note that these differences in probabilities of extinction may be related to any of the model differences discussed in this subsection's first paragraph or parameter value differences. As discussed above, high probabilities of extinction may limit surviving outbreaks to more severe outbreaks. As the pull towards extinction weakens, a larger variety of outbreaks may survive. Recall that, while most SSE-dominated outbreaks are less severe than non-SSE-dominated outbreaks for NHQ ($\kappa \in [0, 1]$), RHQ ($\kappa \in [0, 1]$), and IHQ ($\kappa \in [0.7, 1]$), the most severe SSE-dominated outbreaks are more severe than the most severe non-SSE-dominated outbreaks; this implies that, if sufficiently many of the less severe SSE-dominated outbreaks were to go extinct, most of the surviving SSE-dominated outbreaks may be more severe than the non-SSE-dominated outbreaks, which would agree with the Lloyd, et al.'s, James, et al.'s, and our results for IHQ ($\kappa \in [0, 0.7)$). Overall, differences between the individual-based and event-based models suggest that, if outbreaks are SI- and/or SSE-dominated, SIs and SSEs must be considered separately, as they have distinct influences on outbreak dynamics.

5. Conclusion

To accomplish the main goals of our study (Section 1), we incorporated SSEs into a continuous-time Markov chain (CTMC) model (Section 2.2), imposed a constancy condition (Section 2.3), simulated the CTMC model under multiple scenarios (Section 2.4), and varied quarantine violation levels (Section 2.4). When hospitalization and quarantine are excluded or when hospitalization, quarantine, premature hospital discharge, and quarantine violation are included (either no control or imperfect control), SSE-dominated outbreaks are more variable, less severe, and more likely to go extinct than non-SSE-dominated outbreaks. While most SSE-dominated outbreaks are less severe, the most severe SSE-dominated outbreak is more severe than the most severe non-SSE-dominated outbreaks. When hospitalization and quarantine are included but premature hospital discharge and quarantine violation are excluded (perfect control), SSE-dominated outbreaks are more likely to go extinct than non-SSE-dominated outbreaks but less variable and more severe. When hospitalization, quarantine, premature hospital discharge, and quarantine violation are included and quarantine violation is halved, SSE-dominated outbreaks behave similarly to when hospitalization and quarantine are included but premature hospital discharge and quarantine violation are excluded; when quarantine violation is doubled, outbreaks behave similarly to when hospitalization and quarantine are excluded.

In all scenarios, hospitalization and quarantine are more effective at controlling SSE-dominated outbreaks than non-SSE-dominated outbreaks. Similarly, premature hospital discharge and quarantine violation are more consequential for SSE-dominated outbreaks. When hospitalization and quarantine are excluded, SSE-dominated outbreaks are highly unlikely to go extinct; when hospitalization, quarantine, premature hospital discharge, and quarantine violation are included, SSE-dominated outbreaks are moderately unlikely to go extinct; and when hospitalization and quarantine are included but premature hospital discharge and quarantine violation are excluded, SSE-dominated outbreaks are highly likely to go extinct. Halving quarantine violation approximately doubles the likelihood that SSE-dominated outbreaks go extinct, while doubling quarantine violation approximately halves the likelihood that SSE-dominated outbreaks go extinct.

Altogether, SSE-dominated outbreaks notably differ from non-SSE-dominated outbreaks in terms of variability, severity, and likelihood of

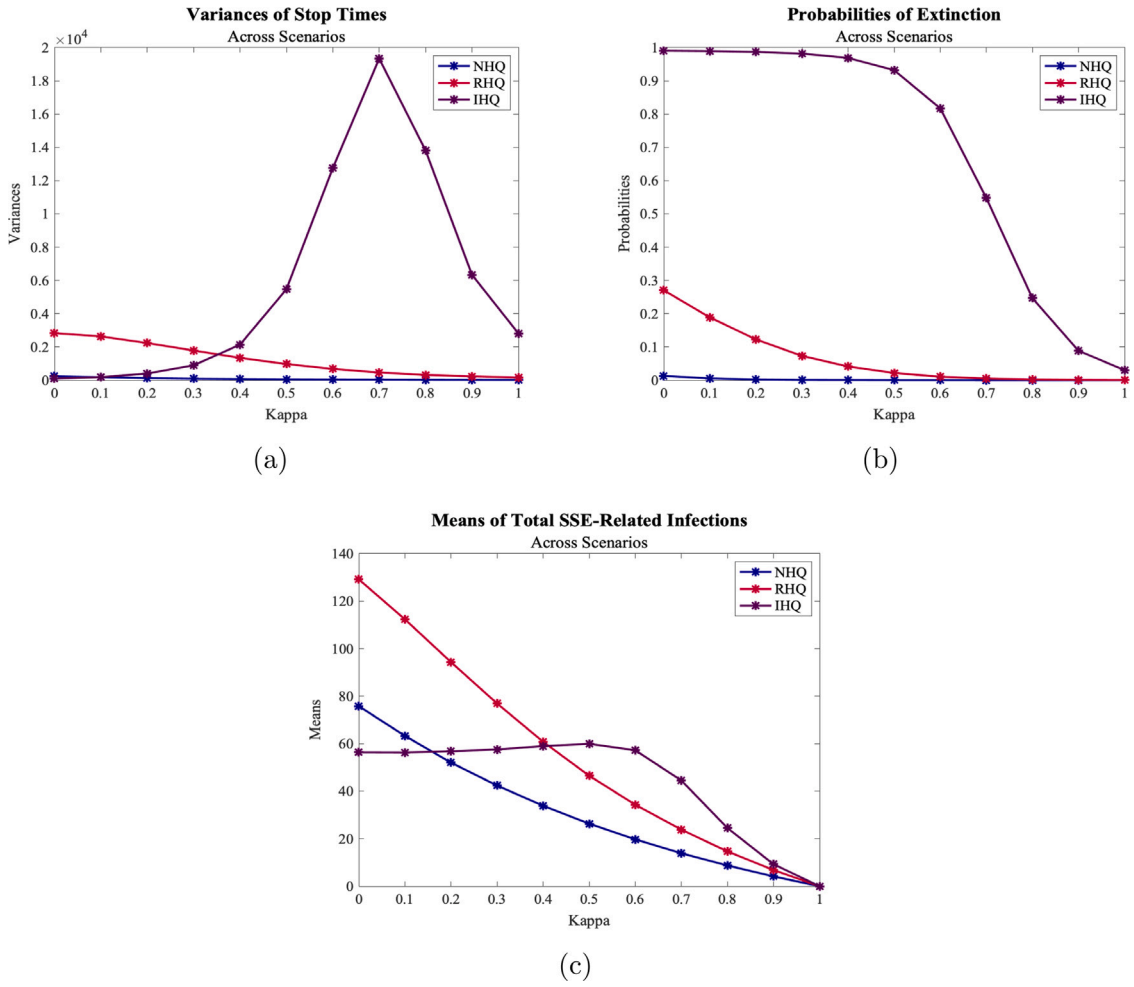

Fig. 6. (a) Variances of stop times across scenarios (b) Probabilities of extinction across scenarios (c) Means of total cumulative SSE-related infections across scenarios.

extinction; they also differ from SI-dominated outbreaks, albeit more subtly (see Section 4). SSE-dominated outbreaks' dynamics are strongly influenced by whether individuals may be hospitalized or quarantined, as well as whether they may be prematurely discharged from the hospital or violate quarantine. Both hospitalization and quarantine are highly effective control measures for SSE-dominated outbreaks, but premature hospital discharge and quarantine violation substantially reduce their effectiveness. Note that we evaluated control measures using the likelihood of extinction. All of the aforementioned has important public health implications (see Section 4), which necessitates that SARS-CoV-2 modelers (1) determine the extent to which SSEs and/or SIs contribute to spread and (2) distinguish between SSEs, SIs, and non-SSEs/non-SIs in their models. Finally, further exploration of the individual and combined influences of SSEs and SIs on outbreak dynamics, as well as the effectiveness of control measures for different types of outbreaks, is necessary to better inform containment and eradication efforts.

CRediT authorship contribution statement

Jordan Bramble: Formal analysis, Visualization, Simulation codes, Writing – original draft, Reviewing and editing. **Alexander Fulk:** Conceptualization, Formal analysis, Writing – review & editing. **Raul Saenz:** Conceptualization, Writing – review & editing. **Folashade B. Agusto:** Conceptualization, Methodology, Project administration, Supervision, Writing – review & editing, Funding acquisition.

Declaration of competing interest

The authors declare that they have no known competing financial interests or personal relationships that could have appeared to influence the work reported in this paper.

Data availability

All data used in this study came from published, cited sources, and are included in the text.

Acknowledgments

This research is supported by National Science Foundation, United States under the grant number DMS 2028297.

Appendix A. Margins of error

Let $\bar{x}$ be the sample mean, $\hat{\sigma}$ be the sample standard deviation, and n be the sample size. Then the 95% confidence interval for $\bar{x}$ is given by $(\bar{x} - z_{0.025}\frac{\hat{\sigma}}{\sqrt{n}}, \bar{x} + z_{0.025}\frac{\hat{\sigma}}{\sqrt{n}})$; $\pm z_{0.025}\frac{\hat{\sigma}}{\sqrt{n}}$ is called the margin of error. Table 3 gives the margins of error for the means of stop times' 95% confidence intervals. The margins of error are small relative to the means of stop times; all 95% confidence intervals are tight and non-overlapping.

Note that the 95% confidence interval formula assumes normality. This is reasonable because, while stop times' distributions are not

Table 3
Margins of error for the means of the stop times' 95% confidence intervals for NQH, RHQ, IHQ, RHQ_{lqv}, and RHQ_{hqv} for $\kappa \in [0,1]$.

Scenario	$\kappa = 0$	$\kappa = 0.1$	$\kappa = 0.2$	$\kappa = 0.3$	$\kappa = 0.4$	$\kappa = 0.5$	$\kappa = 0.6$	$\kappa = 0.7$	$\kappa = 0.8$	$\kappa = 0.9$	$\kappa = 1$
NQH	±0.1337	±0.1143	±0.099	±0.0845	±0.0725	±0.063	±0.0552	±0.0482	±0.0427	±0.0379	±0.0338
RHQ	±0.1474	±0.1424	±0.1311	±0.1172	±0.1015	±0.2735	±0.2283	±0.1884	±0.1568	±0.1337	±0.1127
IHQ	±0.0875	±0.1194	±0.1756	±0.2622	±0.1282	±0.205	±0.1807	±0.2226	±0.1881	±0.2207	±0.1471
RHQ_{lqv}	±0.1743	±0.1884	±0.191	±0.1787	±0.1564	±0.1309	±0.1061	±0.2684	±0.2127	±0.1696	±0.1402
RHQ_{hqv}	±0.3393	±0.3177	±0.2916	±0.2589	±0.2294	±0.1995	±0.1721	±0.147	±0.1254	±0.1075	±0.091

normal, they are light-tailed and only slightly skewed. This, in conjunction with the "approximate" confidence intervals' tightness about stop times' means, suggests the "true" confidence intervals would also be non-overlapping.

Appendix B. Additional figures

See Fig. 6.

References

Agusto, Folashade B., Erovenko, Igor V., Fulk, Alexander, Abu-Saymeh, Qays, Romero-Alvarez, Daniel, Ponce, Joan, Sindi, Suzanne, Ortega, Omayra, Saint Onge, Jarron M., Peterson, A. Townsend, 2022. To isolate or not to isolate: The impact of changing behavior on COVID-19 transmission. BMC Public Health 22 (1), 1–20.

Agusto, Folashade B., Numfor, Eric, Srinivasan, Karthik, Iboi, Enahoro, Fulk, Alexander, Saint Onge, Jarron M., Peterson, Townsend, 2021. Impact of public sentiments on the transmission of COVID-19 across a geographical gradient. MedRxiv.

Alltucker, Ken, Bajak, Aleszu, 2020. 'We're not winning this battle': Relentless COVID-19 surge fills 1 in 8 hospital ICU units. https://www.usatoday.com/story/news/health/2020/12/12/hospitals-lack-icu-bed-space-nation-waits-covid-vaccine/3893339001/. Accessed May 23, 2021.

Althouse, Benjamin M., Wenger, Edward A., Miller, Joel C., Scarpino, Samuel V., Allard, Antoine, Hébert-Dufresne, Laurent, Hu, Hao, 2020. Superspreading events in the transmission dynamics of SARS-CoV-2: Opportunities for interventions and control. PLoS Biol. 18 (11), e3000897.

Antia, Rustom, Regoes, Roland R., Koella, Jacob C., Bergstrom, Carl T., 2003. The role of evolution in the emergence of infectious diseases. Nature 426 (6967), 658–661.

Ashworth, Simon, 2021. Effectiveness of public health measures against covid-19: ventilation has a major role. Bmj 375.

Badu, Kingsley, Oyebola, Kolapo, Zahouli, Julien Z.B., Fagbamigbe, Adeniyi Francis, de Souza, Dziedzom K., Dukhi, Natisha, Amankwaa, Ebenezer F., Tolba, Mai F., Sylverken, Augustina A., Mosi, Lydia, et al., 2021. SARS-CoV-2 viral shedding and transmission dynamics: implications of WHO COVID-19 discharge guidelines. Front. Med. 8.

Bar-Ilan University, 2018. Continuous-Time Markov Chains. https://u.math.biu.ac.il/~amirgi/CTMCnotes.pdf.

Centers for Disease Control and Prevention, 2001. Updated guidelines for evaluating surveillance systems. https://www.cdc.gov/mmwr/preview/mmwrhtml/rr5013a1.htm. Accessed Jun. 6, 2022.

Centers for Disease Control and Prevention, 2021a. Potential rapid increase of omicron variant infections in the United States. https://www.cdc.gov/coronavirus/2019-ncov/science/forecasting/mathematical-modeling-outbreak.html. Accessed Feb. 5, 2022.

Centers for Disease Control and Prevention, 2021b. Public health surveillance. https://www.cdc.gov/csels/dsepd/ss1978/lesson5/appendixa.html. Accessed Jan. 17, 2022.

Centers for Disease Control and Prevention, 2022. CDC COVID data tracker. https://covid.cdc.gov/covid-data-tracker/#datatracker-home. Accessed Feb. 4, 2022.

Centers for Disease Prevention and Control, 2020. COVID-19 pandemic planning scenarios. https://www.cdc.gov/coronavirus/2019-ncov/hcp/planning-scenarios.html. Accessed August 8, 2020.

Chen, Paul Z., Koopmans, Marion, Fisman, David N., Gu, Frank X., 2021. Understanding why superspreading drives the COVID-19 pandemic but not the H1N1 pandemic. Lancet Infect. Dis. 21 (9), 1203–1204.

Cheng, H.-U., Jian, S.-W., Liu, D.-P., Ng, T.-V., Huang, W.-T., Lin, H.-H., 2020. Contact tracing assessment of COVID-19 transmission dynamics in Taiwan and risk at different exposure periods before and after symptom onset. JAMA Internal Med. 180 (9), 1156–1163.

Du, Zhanwei, Wang, Chunyu, Liu, Caifen, Bai, Yuan, Pei, Sen, Adam, Dillon C., Wang, Lin, Wu, Peng, Lau, Eric H.Y., Cowling, Benjamin J., 2022. Systematic review and meta-analyses of superspreading of SARS-CoV-2 infections. Transbound. Emerg. Dis..

Edholm, Christina J., Levy, Benjamin, Spence, Lee, Agusto, Folashade B., Chirove, Faraimunashe, Chukwu, Chidozie W., Goldsman, David, Kgosimore, Moatlhodi, Maposa, Innocent, White, Jane K.A., et al., 2022. A vaccination model for COVID-19 in Gauteng, South Africa. Infect. Dis. Model..

Gabbat, Adam, Laughland, Oliver, 2022. Hospitals in half of US states close to capacity as Omicron continues surge. https://www.theguardian.com/us-news/2022/jan/14/us-hospitals-capacity-staffing-shortages-omicron-covid. Accessed Jun. 5, 2022.

Gillespie, Daniel T., 1976. A general method for numerically simulating the stochastic time evolution of coupled chemical reactions. J. Comput. Phys. 22 (4), 403–434.

Haischer, Michael H., Beilfuss, Rachel, Hart, Meggie Rose, Opielinski, Lauren, Wrucke, David, Zirgaitis, Gretchen, Uhrich, Toni D., Hunter, Sandra K., 2020. Who is wearing a mask? Gender-, age-, and location-related differences during the COVID-19 pandemic. PLoS One 15 (10), e0240785.

Hernandez, David, 2020. Citations issued across san diego county for violations of stay-home order reach 125. https://www.sandiegouniontribune.com/news/public-safety/story/2020-04-15/citations-issued-across-san-diego-county-for-violations-of-stay-home-order-reach-125. Accessed May 23, 2021.

Hoeben, Evelien M., Bernasco, Wim, Suonperä Liebst, Lasse, Van Baak, Carlijn, Rosenkrantz Lindegaard, Marie, 2021. Social distancing compliance: A video observational analysis. PLoS One 16 (3), e0248221.

Hubbard, Kaia, 2022. Hospitals nearing capacity in majority of states as Omicron surges. https://www.usnews.com/news/health-news/articles/2022-01-14/hospitals-nearing-capacity-in-majority-of-states-as-omicron-surges#:~:text=Home-,Hospitals%20Nearing%20Capacity%20in%20Majority%20of%20States%20as%20Omicron%20Surges,Skyrocket%2C%20according%20to%20new%20data.&text=By%20Kaia%20Hubbard-,Jan.,2022%2C%20at%2012%3A30%20p.m. Accessed Jun. 5, 2022.

James, Alex, Pitchford, Jonathan W., Plank, Michael J., 2007. An event-based model of superspreading in epidemics. Proc. R. Soc. B 274 (1610), 741–747.

Jamison, Dean T, Gelband, Hellen, Horton, Susan, Jha, Prabhat, Laxminarayan, Ramanan, Mock, Charles N., Nugent, Rachel, 2018. Disease Control Priorities: Improving Health and Reducing Poverty. International Bank for Reconstruction and Development / The World Bank, Washington, D.C..

Johansson, Michael A., Quandelacy, Talia M., Kada, Sarah, Prasad, Pragati Venkata, Steele, Molly, Brooks, John T., Slayton, Rachel B., Biggerstaff, Matthew, Butler, Jay C., 2021. SARS-CoV-2 transmission from people without COVID-19 symptoms. JAMA Netw. Open 4 (1), e2035057.

Keeling, Matt J., Rohani, Pejman, 2008. Modeling Infectious Diseases in Humans and Animals. Princeton University Press, Princeton, NJ.

Knight, Cameron, 2020. Violating stay-at-home order: 66 now face charges in Hamilton County. https://www.cincinnati.com/story/news/2020/04/17/violating-stay-home-order-59-now-face-charges-hamilton-county/5151433002/. Accessed May 23, 2021.

KSTP, 2020. 25 Charged with violating Minnesota's 'stay at home' order. https://kstp.com/coronavirus/25-charged-with-violating-minnesotas-stay-at-home-order-april-14-2020/5700505/. Accessed May 23, 2021.

Lakdawala, Seema S., Menachery, Vineet D., 2021. Catch me if you can: superspreading of COVID-19. TIM 29 (10), 919–929.

Lloyd-Smith, James O., Schreiber, Sebastian J., Kopp, P. Ekkehard, Getz, Wayne M., 2005. Superspreading and the effect of individual variation on disease emergence. Nature 438 (7066), 355–359.

Maxmen, Amy, 2021. Has COVID taught us anything about pandemic preparedness? Nature 332–335.

McCarthy, Niall, 2020. Many U.S. hospitals are running critically short of ICU beds [Infographic]. https://www.forbes.com/sites/niallmccarthy/2020/12/10/many-us-hospitals-are-running-critically-short-of-icu-beds-infographic/?sh=72c97eaf65fe. Accessed May 23, 2021.

MIDAS Network, 2021. Parameter estimates for 2019 novel coronavirus. https://github.com/midas-network/COVID-19/tree/master/parameter_estimates/2019_novel_coronavirus. Accessed: 2021-06-15.

Miller, Joel C., 2018. A primer on the use of probability generating functions in infectious disease modeling. Infect. Dis. Model. 3, 192–248.

MultiState Policy Team, 2021. COVID-19 policy tracker. https://www.multistate.us/issues/covid-19-policy-tracker. Accessed Feb. 4, 2022.

Mushanyu, Josiah, Chukwu, Williams, Nyabadza, Farai, Muchatibaya, Gift, 2022. Modelling the potential role of super spreaders on COVID-19 transmission dynamics. Int. J. Math. Model. Numer. Optim. 12:2, 191–209.

Ndaïrou, Faïçal, Area, Iván, Nieto, Juan J., Torres, Delfim F.M., 2020. Mathematical modeling of COVID-19 transmission dynamics with a case study of wuhan. Chaos Solitons Fractals 135, 109846.

Oluwatobilloba, Ige, 2020. Markov Chain Epidemic Models and Parameter Estimation (Ph.D. thesis). Marshall University Mathematics Department, Huntington, WV.

Our World in Data, 2020. COVID-19: Stay-at-home restrictions. https://ourworldindata.org/covid-stay-home-restrictions. Accessed May 23, 2021.

Pokora, Roman, Kutschbach, Susan, Weigl, Matthias, Braun, Detlef, Epple, Annegret, Lorenz, Eva, Grund, Stefan, Hecht, Juergen, Hollich, Helmut, Rietschel, Peter, et al., 2021. Investigation of superspreading COVID-19 outbreak events in meat and poultry processing plants in Germany: A cross-sectional study. PLoS One 16 (6), e0242456.

Queen's University, 2005. Continuous-Time Markov Chains - Introduction. https://mast.queensu.ca/~stat455/lecturenotes/set5.pdf.

Renardy, Marissa, Eisenberg, Marisa, Kirschner, Denise, 2020. Predicting the second wave of COVID-19 in Washtenaw county, MI. J. Theor. Biol. 507, 1–20.

Sanche, S., Lin, Y., Xu, C., Romero-Severson, E., Hengartner, N., Ke, R., 2020. High contagiousness and rapid spread of severe acute respiratory syndrome coronavirus 2. Emerg. Infect. Dis. 26 (7), 1470–1477.

Shakiba, Nika, Edholm, Christina J., Emerenini, Blessing O., Murillo, Anarina L., Peace, Angela, Saucedo, Omar, Wang, Xueying, Allen, Linda J.S., 2021. Effects of environmental variability on superspreading transmission events in stochastic epidemic models. Infect. Dis. Model. 6, 560–583.

Swinkels, Koen, 2020. SARS-CoV-2 superspreading events database. https://kmswinkels.medium.com/covid-19-superspreading-events-database-4c0a7aa2342b. Accessed December 1, 2020.

Thompson, R.N., Gilligan, C.A., Cunniffe, N.J., 2020. Will an outbreak exceed available resources for control? Estimating the risk from invading pathogens using practical definitions of a severe epidemic. J. R. Soc. Interface 17 (172), 20200690.

UK Health Security Agency, 2022. Research and analysis COVID-19 confirmed deaths in England (to 31 January 2021): report. https://www.gov.uk/government/publications/covid-19-reported-sars-cov-2-deaths-in-england/covid-19-confirmed-deaths-in-england-report. Accessed June 25, 2022.

University of Cambridge, 2008. Probability Generating Functions. https://Www.Cl.Cam.Ac.Uk/Teaching/0708/Probabilty/Prob06.Pdf.

West Hawaii Today Staff, 2020. More people arrested, cited for violating stay-at-home order. https://www.westhawaiitoday.com/2020/05/21/hawaii-news/more-people-arrested-cited-for-violating-stay-at-home-order/. Accessed May 23, 2021.

Wilasang, Chaiwat, Jitsuk, Natcha C., Sararat, Chayanin, Modchang, Charin, 2022. Reconstruction of the transmission dynamics of the first COVID-19 epidemic wave in Thailand. Sci. Rep. 12 (1), 1–10.

Woolhouse, Mark E.J., Haydon, Daniel T., Antia, Rustom, 2005. Emerging pathogens: the epidemiology and evolution of species jumps. Trends Ecol. Evol. 20 (5), 238–244.

World Health Organization, 2022. WHO coronavirus (COVID-19) dashboard. https://covid19.who.int/. Accessed Feb. 4, 2022.